

Molecular packing and phase transitions of side-chain liquid crystalline polymethacrylates based on *p*-methoxyazobenzene

Xing-Qi Zhu, Jia-Hao Liu, Yi-Xin Liu, Er-Qiang Chen*

Beijing National Laboratory for Molecular Sciences, Department of Polymer Science and Engineering and the Key Laboratory of Polymer Chemistry and Physics of the Ministry of Education, College of Chemistry and Molecular Engineering, Peking University, Beijing 100871, China

ARTICLE INFO

Article history:

Received 29 January 2008
Received in revised form 16 April 2008
Accepted 26 April 2008
Available online 3 May 2008

Keywords:

Side-chain liquid crystalline polymer
Azobenzene
Phase structure

ABSTRACT

The phase structures and transition behaviors of a series of side-chain liquid crystalline (LC) polymethacrylates based on *p*-methoxyazobenzene (PM n Azs, $n = 6, 8, 10, 12$) were studied using differential scanning calorimetry, one- and two-dimensional (1D and 2D) wide-angle X-ray diffraction, and Fourier transform infrared spectroscopic experiments. The LC phase transition of PM n Az follows the sequence of smectic A (SmA) \leftrightarrow nematic (N) \leftrightarrow isotropic (I). For PM10Az and PM12Az, the transition of SmA-to-N is not complete upon heating. In the low-temperature SmA phase, the polymers adopt a fully interdigitated side-chain packing with the smectic layer period almost identical to the side-chain length. For all the four samples, the first-order diffraction of the SmA structure only renders when the temperature approaches the transition of SmA \leftrightarrow N, with the intensity much lower than that of the second-order diffraction. The absence of the first-order diffraction at low temperatures is ascribed to the possible matching of the electron densities between the center portion of the side-chain sublayer and the main-chain sublayer of the SmA structure. Since only the mesogens from the same main-chain sublayer can stack parallel together, the distribution of the azobenzene domains may cause some sort of density undulation within the smectic layer. Among the samples, PM6Az presents the strongest undulation with some additional orders. We also examined the annealing effect on the H-aggregation of PM n Azs. It is found that isothermal annealing at a temperature slightly higher than the T_g of PM8Az and PM10Az can significantly enhance the UV absorption at 326 nm, indicating a further development of H-aggregation. However, for PM6Az and PM12Az, the UV-vis spectrum of the annealed sample is nearly identical to that without annealing.

© 2008 Elsevier Ltd. All rights reserved.

1. Introduction

Azobenzene chromophore is one of the typical functional units which can undergo reversible *trans*–*cis* isomerization under photoirradiation. Numerous efforts have been endeavored to incorporate azobenzene moieties into polymers, with the aim to explore their great potential applications in optical switching, optical data storage, polarization holography, soft actuators as artificial muscles, and so forth [1–12]. As the rodlike *trans*-azobenzene is also a typical mesogenic unit, the azobenzene containing side-chain polymers usually display the liquid crystalline (LC) phase behaviors. It has been revealed that the performance of the functional polymers with azobenzenes is largely related to their LC properties. For instance of soft actuators, compared with the amorphous polymer materials responding to external stimuli in an isotropic way with small deformation, LC elastomers with aligned azobenzene mesogens under actinic light can deform largely in

a preferential direction, and moreover, can respond much faster [13]. For photoorientation behavior, it is reported that the LC polymethacrylates with azobenzene side chains can undergo photoinduced uniaxial and/or biaxial reorientation. The resultant high-optical anisotropy demonstrates excellent thermostability even above the glass transition temperature (T_g), which can be ascribed to the formation of well-ordered LC domains or H-aggregation of azobenzenes in the film samples [14].

Similar to other side-chain LC polymers, azobenzene containing side-chain LC polymers may form low-ordered LC phases, namely, nematic (N), smectic A (SmA) and C (SmC) phases [15–25]. Their phase structure and transition depend strongly on various factors such as the chemical structure of azobenzene moieties, the spacer length, the tail of side-chain, etc., on which also their photo-responsive behavior relies. For SmA commonly observed in azobenzene side-chain polymers, partially interdigitated SmA phase has been identified. As an example, a series of polymethacrylates with cyanoazobenzene side chains may have the polar mesogens from both main-chain sublayers of the smectic layer to stack parallel with each other [17,18]. On the other hand, monolayer SmA phase with fully interdigitated side-chain packing is readily

* Corresponding author. Tel./fax: +86 010 62753370.
E-mail address: eqchen@pku.edu.cn (E.-Q. Chen).

obtained when the azobenzene moieties are less polar [15]. As the LC properties of the azobenzene side-chain polymers largely impact on their performance as functional materials, careful examination of their phase behavior is necessary.

In the present work, we intend to describe a detail study of the LC behavior of a series of polymethacrylates containing *p*-methoxyazobenzene side chains (PMnAzs with $n = 6, 8, 10, 12$, see Chart 1). The photoresponsive properties of PMnAzs have been extensively investigated [14,26–29]. Although SmA phase is suggested for the polymers at low temperature [14,24,26–29], a complete characterization of their LC behavior particularly based on wide-angle X-ray diffraction (WAXD) method is absent. By combining the experimental results of various techniques, we demonstrate that PMnAz exhibits the phase transition sequence of SmA \leftrightarrow N \leftrightarrow isotropic (I). For PM10Az and PM12Az, the transition of SmA-to-N is not complete upon heating. The low-temperature SmA phase is a monolayer one with fully interdigitated side-chain packing, wherein the backbones of PMnAz form a sublayer squeezed by two adjacent sublayers of side chains. In a wide temperature range below the transition of SmA \leftrightarrow N, the first-order diffraction of the SmA structure is missing, most likely due to the electron density matching between the center portion of the side-chain sublayer and the main-chain sublayer. As only the mesogens from the same main-chain sublayer can stack parallel together, the distribution of the azobenzene domains within the smectic layer causes some sort of density undulation. Among the four samples, PM6Az presents the strongest undulation with some additional orders. It is found that isothermal annealing at a temperature slightly higher than the T_g of PM8Az and PM10Az can significantly enhance the UV absorption at 326 nm, indicating a further development of H-aggregation. However, for other two samples with longer and shorter spacer lengths, annealing does not show considerable impact on the H-aggregation.

2. Experimental section

2.1. Sample preparation

PMnAzs ($n = 6, 8, 10, 12$) were synthesized with conventional free radical polymerization from corresponding monomers according to the literature [30,31]. In brief, the monomer was dissolved in chlorobenzene with a concentration of 25 wt%, and 0.5 mol% 2,2'-azobisisobutyronitrile (AIBN) relative to monomer was added as the initiator. After being degassed with three freeze-thaw cycles, the tube was sealed under vacuum. The polymerization was carried out at 60 °C for 24 h to obtain sufficiently high molecular weight (MW). The resultant polymers were purified by repeated dissolution in THF and precipitation in methanol. After purification, the polymer was dried under vacuum at 40 °C. The chemical structures of monomers and polymers were confirmed by various characterization techniques. The tacticities of PMnAz were evaluated by ^1H NMR according to the literature [32–34]. The apparent number-average MWs (M_n s) and polydispersities (dws) of the polymers were estimated using gel permeation chromatography (GPC, Waters 150C) calibrated with PS standard samples, which are summarized in Table 1.

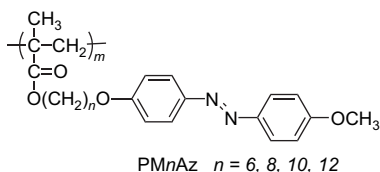


Chart 1. Chemical structure of PMnAz.

Table 1
MW characterization and phase transition parameters of PMnAzs

Sample	$M_n \times 10^{-5a}$ (g/mol)	dw ^a	T_g^b (°C)	T_{S-N} (°C)	ΔH_{S-N} (kJ/mol)	T_{N-I}^b (°C)	ΔH_{N-I} (kJ/mol)
PM6Az	2.01	1.4	75	96 ^b	0.83 ^b	137	1.62 ^b
PM8Az	0.92	1.8	71	117 ^b	1.95 ^b	136	1.82 ^b
PM10Az	1.04	1.9	67	128 ^c	2.83 ^c	136	3.86 ^c
PM12Az	1.20	1.8	64	134 ^c	2.37 ^c	138	5.12 ^c

^a The apparent M_n [(g/mol)] and polydispersity dw were measured by GPC.

^b The glass transition temperature (T_g) and the liquid crystal transition temperatures (T_{S-N} and T_{N-I}) were measured by DSC at a heating rate of 10 °C/min after the samples were cooled from isotropic state and then annealed at ~ 55 °C for 3 h.

^c For PM10Az and PM12Az, the T_{S-N} and the transition enthalpies are estimated from the results of peak deconvolution as shown in Fig. 1, which include some arbitrariness.

2.2. Instruments and experiments

Thermal behaviors of the polymers were examined using a differential scanning calorimetry (DSC). Experiments were performed on a Perkin-Elmer Pyris 1 DSC. The temperature and heat flow at different cooling and heating rates (2.5–20 °C/min) were calibrated using standard materials. The samples were encapsulated in hermetically sealed aluminum pans, with a typical sample weight of ~ 5 mg. Cooling experiment was always conducted before heating experiment. The transition temperatures were determined by measuring the peak temperatures from the heating scans at a rate of 10 °C/min. To separate the overlapped thermal events, peak deconvolution was performed using PeakFit program (Jandel Scientific).

Two-dimensional (2D) WAXD fiber patterns were obtained by using a Bruker D8Discover diffractometer with a 3 kW ceramic tube as the X-ray source (Cu K α) and a GADDS detector. The diffraction peak positions were calibrated with silicon powder ($2\theta > 15^\circ$) and silver behenate ($2\theta < 10^\circ$). The oriented samples prepared by mechanically drawing the fibers in the LC phases were mounted on the sample stage with the fiber axis aligned perpendicular to the point-focused X-ray incident beam. To examine the phase structure change with temperature, the 2D diffraction patterns were recorded in a transmission mode at different temperatures upon heating from room temperature. The background scattering was recorded and subtracted from the sample patterns.

The X-ray diffraction experiments of the fiber samples were also performed with a high-flux small-angle X-ray scattering instrument (SAXSess, Anton Paar) equipped with Kratky block-collimation system and a Philips PW3830 sealed-tube X-ray generator (Cu K α). The one-dimensional (1D) diffraction patterns were recorded on an imaging plate with a pixel size of $42.3 \times 42.3 \mu\text{m}^2$ which extends to the high-angle range (the q range covered by the imaging plate is from 0.06 to 29 nm^{-1} , i.e., the 2θ from 0.08 to 42° with the X-ray wavelength λ of 0.1542 nm). The original experimental data such as data acquisition, background subtraction, and data reduction, were handled by Anton Paar SAXSquant 1.01 software and PCG software package. As the fiber axis of the PMnAz samples was aligned parallel to the line-focused X-ray incident beam, desmearing of the scattering intensity was not further performed. A temperature control unit (Anton Paar TCS300) in conjunction with the SAXSess was utilized to study the structure evolutions as a function of temperature.

UV-vis absorption spectra were recorded on a Perkin-Elmer Lambda35 spectrophotometer, and Fourier transform infrared (FT-IR) spectra were measured on an FT-IR (FTS-65A) with a resolution of 4 cm^{-1} . The film samples were obtained by static casting the THF solutions of PMnAzs with a concentration of $\sim 1 \times 10^{-2}$ g/mL on quartz or KBr plate. To measure the UV-vis absorption change with time during isothermal annealing, the film samples were placed in a Mettler hot stage (FP-90) at a preset temperature.

After a certain period of annealing time, the sample was rapidly transferred to the spectrophotometer at room temperature to record the spectrum. The UV–vis absorption of films annealed at elevated temperatures for 5 min in hot stage was also examined. For the FT-IR heating experiments, the films on KBr substrates were inserted into a sample holder equipped with a built-in heating block, and the samples were stayed isothermally at each temperature for 10 min before measurement.

3. Results and discussion

Fig. 1 shows a set of DSC heating curves of PMnAzs at a rate of 10 °C/min. Before heating, the samples were cooled from 160 °C followed by annealing at ~55 °C for 3 h. As the annealing process induced endothermic hysteresis peak at the glass transition region, the glass transition of the samples at around 70 °C becomes more evident. Taking the temperature where 50% devitrification takes place as the glass transition temperature (T_g), the T_g s of PMnAzs are measured to be slightly decreased with increasing the spacer length (see Table 1). For PM6Az and PM8Az, two endotherms are clearly observed after T_g upon heating, which shall be associated with two first-order transitions. For PM10Az and PM12Az, careful examination reveals that a broad and relatively weak transition exists right before the major one, as shown by the deconvolution results plotted in Fig. 1 (see the red dashed curves). The onsets of the transitions above T_g exhibit little cooling or heating rate dependence, which features the transitions of LC phases. Using PM6Az as an example, Fig. 2 describes a set of DSC cooling and subsequent heating thermal diagrams at different rates (2.5–20 °C/min). After extrapolating to 0 °C/min, the onset of the highest transition of PM6Az upon cooling was estimated to be 137 °C. With this value as the reference, the undercooling dependence is found to be within 1 °C when the cooling rate varies from 2.5 to 20 °C/min, meaning that the transition is close to thermodynamic equilibrium. The temperatures (peak temperatures observed on the DSC heating traces with a rate of 10 °C/min) and enthalpies of transitions of the four samples are summarized in Table 1.

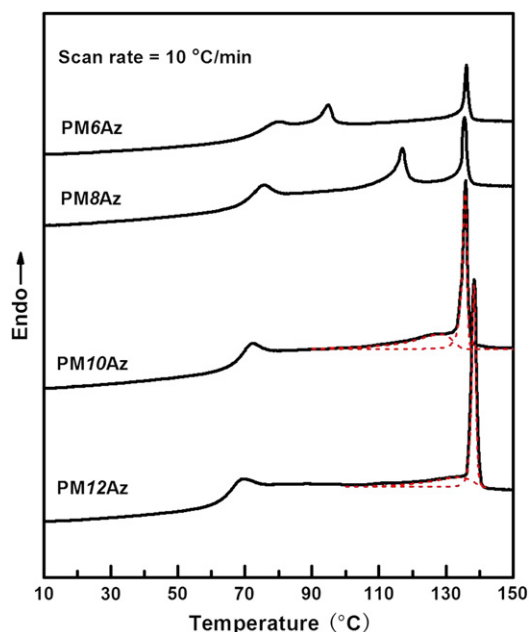


Fig. 1. DSC heating traces of PMnAzs at 10 °C/min. Before heating, the PMnAz samples were cooled from 160 °C at 10 °C/min and then annealed at ~55 °C for 3 h. The red dashed curves represent the deconvolution results of the endothermic events of PM10Az and PM12Az. (For interpretation of the references to colour in this figure legend, the reader is referred to the web version of this article.)

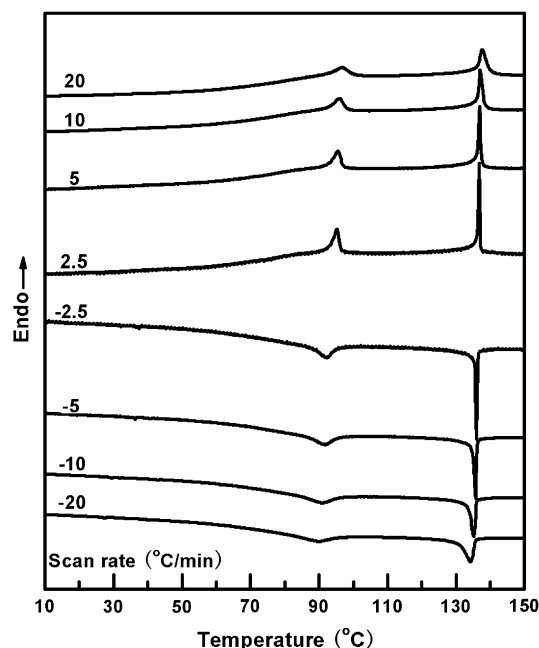


Fig. 2. Set of DSC curves of PM6Az at different cooling and heating rates.

According to the chemical structure of PMnAzs with the side chains containing *p*-methoxyazobenzene, one may consider that the low-temperature LC phase can be an SmA [24,29], and the transitions follow the sequence of SmA \leftrightarrow N \leftrightarrow I. Since the two transitions of both PM6Az and PM8Az are well separated, it is easy to confirm that the high-temperature transition was associated with N \leftrightarrow I by using WAXD experiments. Fig. 3a and b depicts two 2D WAXD patterns of PM8Az recorded with the X-ray incident beam perpendicular to the fiber direction at 125 and 140 °C, respectively. The oriented sample was obtained by mechanical spinning at 115 °C followed by quenching to room temperature. From Fig. 3a (125 °C), we observe that a pair of high-angle scattering with the intensity maximum at 2θ of ~19.4°, which in side-chain polymer is mainly due to the lateral interferences between side groups, is more or less concentrated on meridian (the fiber direction). On the other hand, a pair of diffused halo with broad azimuthal distribution is located at 2θ of ~7.0° in the low-angle region. This pattern indicates that the orientation of the chain backbone and also the mesogens on side-chain is remained when the temperature exceeds the low endotherm peaked at 117 °C, featuring an N phase of PM8Az. Further heating the sample would result in an N-to-I transition. At 140 °C, only a ring pattern is observed (Fig. 3b), indicating that the molecular orientation is completely lost and thus the sample becomes isotropic.

For PM10Az and PM12Az, the broad low-temperature transition overlaps with the major one as shown by the DSC curves in Fig. 1. During heating, the diffraction from a smectic structure gradually decreased in intensity when the temperature entered the low-transition range. A typical 2D WAXD pattern for N phase of PM10Az could be caught at the temperature right below the major transition. However, the heating experiment of PM12Az fiber elucidated that before the 2D WAXD pattern became complete isotropic, the residual of the smectic diffraction could be observed, indicating that the transition from SmA-to-N was not complete. Consequently, as shown in Table 1, the enthalpy of the major transition of PM12Az becomes much higher in comparison with those of PM6Az and PM8Az which are typical for N-to-I transition of side-chain LC polymers [35,36]. For PM10Az, the enthalpy of the major transition is lower than that of PM12Az but considerably

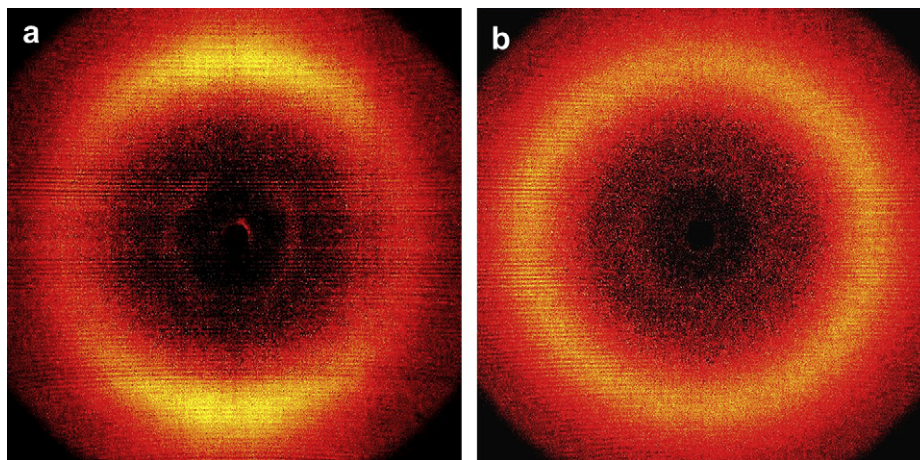


Fig. 3. 2D WAXD fiber patterns of PM8Az recorded at 125 (a) and 140 °C (b). The fiber axis is along meridian.

higher than that of the other two polymers. This may be also ascribed to the incomplete transition of SmA-to-N prior to the major transition of PM10Az.

Although an SmA structure is a reasonable hypothesis for PMnAzs, to realize the detail molecular packing of the polymers demands more careful WAXD experiments. We found that PMnAzs ($n = 8, 10, 12$) shared the same diffraction feature at room temperature, but the 2D WAXD pattern of PM6Az looks different. We will discuss their diffraction patterns separately below.

The 2D WAXD patterns of PMnAz ($n \geq 8$) recorded at 25 °C with the X-ray incident beam perpendicular to the fiber direction are shown in Fig. 4. The diffraction patterns feature an SmA structure. In the high 2θ region, a pair of amorphous halos with the scattering maximum at $\sim 21.0^\circ$ is located on meridian (the fiber direction). On the other hand, a pair of sharp low-angle spots, which should be correlated to the smectic layer diffraction, appears on equator. As the chain backbones are aligned along meridian, this diffraction pattern indicates that the mesogenic groups on side chains are parallel to the smectic layer normal. However, it is surprising to note that for all the three samples, the sharp low-angle diffraction on equator only corresponds to a d spacing of a half of the side-chain length estimated with an assumption that the alkyl spacer adopts an all-*trans* conformation. For example, the d spacing of the low-angle diffraction of PM8Az is measured to be 1.34 nm; but the calculated side-chain length is 2.82 nm. This observation implies that the electron density profile along the smectic layer normal or side-chain packing is different from that usually found in SmA phases of side-chain LC polymers.

We further examined the diffraction of the fiber PMnAz ($n \geq 8$) samples at room temperature by using SAXSess with a high-resolution imaging plate as detector. Since we aligned the fiber direction of PMnAzs ($n \geq 8$) parallel to the line-focused X-ray incident beam of SAXSess, the diffractions recorded on the imaging plate are along the layer normal to the SmA. As indicated by the arrows in Fig. 5, more low-angle diffraction peaks can be observed with increasing the spacer length, wherein the first diffractions locate at the 2θ angles identical to those shown in Fig. 4a–c for $n = 8, 10, 12$, respectively. Interestingly, the scattering vectors of the multiple peaks are found to follow a ratio of 2:3:4 rather than that of 1:2:3. Therefore, we presume that the first-order diffraction of the smectic layer, which shall correspond to the full side-chain length, is missing at room temperature.

We found that the missed first-order diffraction could be observed upon our WAXD heating experiments of PMnAzs ($n \geq 8$). As an example, Fig. 6 presents a set of 1D WAXD patterns of a PM10Az fiber at different temperatures recorded using SAXSess. Again, the fiber direction was aligned parallel to the X-ray line-focused beam. During the heating experiment, only two sharp diffractions at 5.7° and 8.6° are observed at below 90°C . Afterwards, a new diffraction peak can be unambiguously identified at a 2θ of 2.9° , i.e., the corresponding d spacing of the peak is almost identical to the calculated side-chain length of 3.07 nm. As no peak at a 2θ angle lower than 2.9° can be detected, we assign this new peak to be the first-order diffraction of the SmA of PM10Az. In our 2D WAXD results of PMnAzs ($n \geq 8$) (Fig. 7), we further identify that the first-order diffraction is located on equator,

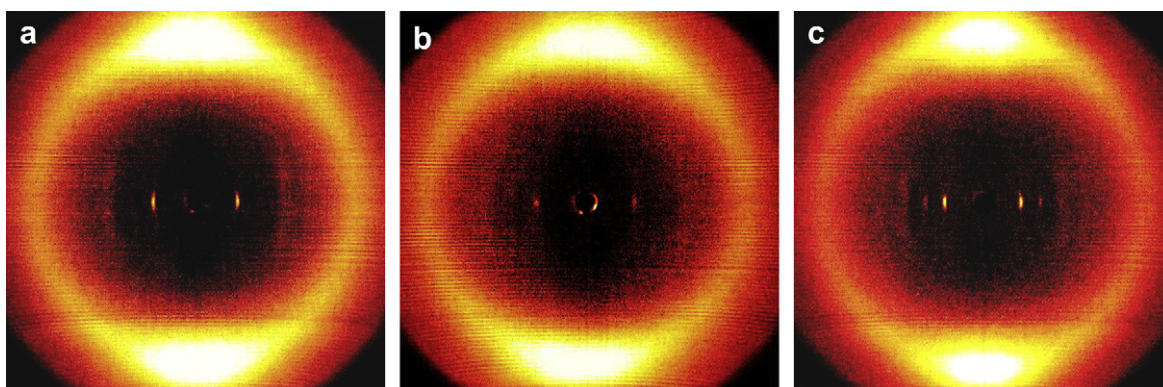


Fig. 4. 2D WAXD fiber patterns of PMnAzs with $n = 8$ (a), 10 (b), and 12 (c) at 25 °C. The samples were obtained by spinning at the smectic state. The X-ray incident beam was perpendicular to the fiber direction which is along the meridian.

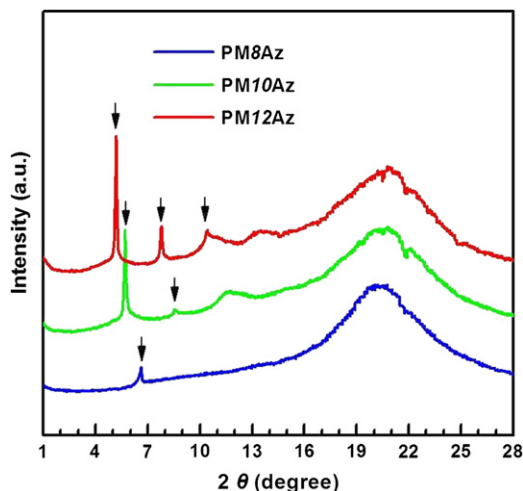


Fig. 5. 1D WAXD patterns of PM n Az ($n = 8, 10, 12$) recorded by SAXSess at 25 °C. The samples were oriented by spinning and then mounted on the sample holder with the line-focused X-ray incident beam parallel to the fiber direction.

confirming the LC phase of SmA. Although the first-order diffraction is rather weaker than the second order one, its sharpness reflects that the SmA phase is well developed, namely, an apparent correlation length of ~ 110 nm along the smectic layer normal can be estimated by using the Scherrer equation.

The diffraction behavior of PM6Az needs an additional discussion. Fig. 8a shows a 2D WAXD pattern recorded at 25 °C of a PM6Az fiber spun at 125 °C, wherein the fiber axis is along meridian. In the high-angle region, a pair of strong scattering halos is observed to be concentrated on meridian, indicating that the sample is well oriented. However, in the low-angle region, four rather diffuse spots with 2θ of $\sim 8.4^\circ$ are located in quadrants, which imply some characteristics of an SmC structure. The projection of the spots on equator corresponds to a d spacing of

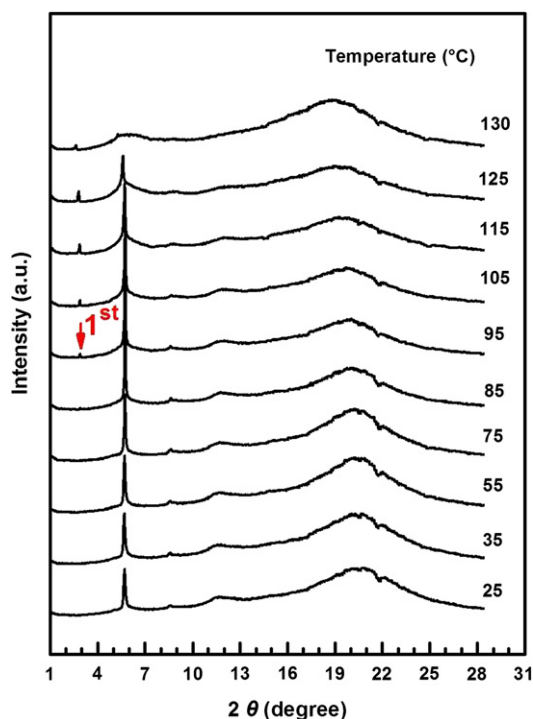


Fig. 6. A set of 1D WAXD patterns of a PM10Az fiber recorded using SAXSess at different temperatures upon heating.

a half of the calculated side-chain length (2.46 nm), inferring again that the first-order diffraction is absent. The diffraction of the fiber annealed at 85 °C is described in Fig. 8b. Compared with the pattern of Fig. 8a, the low-angle spots in quadrants become concentrated, and more importantly, a pair of sharp diffractions at 2θ of 3.5° (i.e., d spacing of 2.55 nm) that shall be the first-order diffraction appears on equator. As another pair of arcs on the equator with a d spacing of 0.83 nm can be assigned as the third order diffraction, most likely, PM6Az also forms an SmA structure. The quadrant scattering may be due to some sort of density undulation within the smectic layers [25,37].

On the basis of the WAXD experimental results, we consider that all the four PM n Az samples shall have an SmA phase at low temperature. Since the periodicity of the SmA layer is completely determined by the side-chain length, the SmA structure shall be a monolayer with fully interdigitated side-chain packing. As illustrated schematically in Fig. 9, the backbones of poly(methacrylate) incompatible with the side chains form a sublayer squeezed by two adjacent side-chain sublayers [15,20,25]. According to the chemical structure of the side chains, we suggest that only the azobenzenes emanating from the same main-chain sublayer are allowed to stack parallel with each other, resulting in many small mesogen domains within the SmA layer (see the parts indexed by boxes with dashed line in Fig. 9). Consequently, the mesogen interaction is not maximized. However, if the azobenzenes from both sides are stacked parallel with each other to form a complete mesogen sublayer at the center of the SmA layer, the density of the space filled by the non-polar spacers will be impractically low. Therefore, this fully interdigitated side-chain packing scheme shall be mainly due to that the density of smectic layer is prone to be uniform as much as possible.

The absence of the first-order diffraction at low temperature suggests that the electron density at the center portion of the side-chain sublayer (ρ_{center}) is very close to that of the main-chain sublayer ($\rho_{\text{main-chain}}$), and thus is lower than the domains containing azobenzene groups (see Fig. 9) [38]. Heating to high temperature can increase the difference between ρ_{center} and $\rho_{\text{main-chain}}$, resulting in the appearance of the first-order diffraction. Fig. 10 shows a set of FT-IR spectra of PM8Az films obtained at different temperatures upon heating. The 1472 cm^{-1} band can be assigned as $-gtmg'$ -type with a *trans*-dominated (m , large) conformation of the alkyl spacer, whereas the 1467 cm^{-1} band is associated with a *gauche*-dominated conformation (m , small) [39]. With increasing temperature, the band at 1467 cm^{-1} gradually becomes more intense than that at 1472 cm^{-1} , revealing that the alkyl spacers adopted more *gauche* conformation. This conformational change can result in a slight decrease of the average side-chain length. Therefore, the mesogen domains on right and left side within the SmA layer become closer, and the ρ_{center} should be increased accordingly. On the other hand, the inevitable thermal expansion will decrease the $\rho_{\text{main-chain}}$, particularly when the chains become quite mobile at the temperatures higher than T_g . These two opposite tendencies may finally result in sufficiently large density difference between ρ_{center} and $\rho_{\text{main-chain}}$ at high temperature.

As mentioned above, the second order diffractions of PM6Az appeared in quadrants may reflect a sort of density undulation within the smectic layers. In fact, similar density undulation may also exist in PM n Az ($n \geq 8$), although it is not as strong as that in PM6Az. From the 2D WAXD results in Fig. 7, we can observe that the second order diffractions of PM n Az ($n \geq 8$) are all diffused into the quadrants. This density undulation probably arises from the distribution of the mesogen domains within the smectic layers. It is well known that conventional radical polymerization can result in the poly(methacrylate) derivatives with rather high content of rr triad stereosequences. According to our ^1H NMR results (see Supporting information), the [mm], [mr], and [rr] of PM6Az were

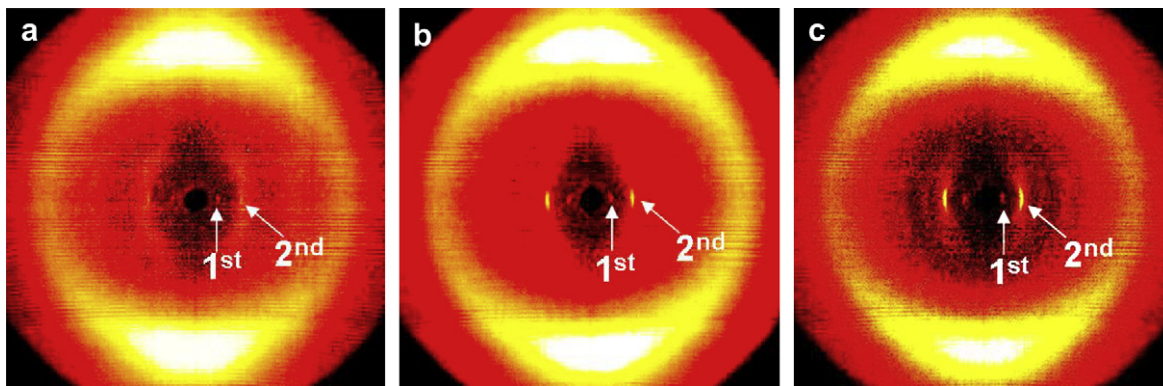


Fig. 7. 2D WAXD patterns of PMnAzs with $n=8$ (a), 10 (b), and 12 (c) at 110 °C. The arrows in the patterns indicate the first and second order diffractions.

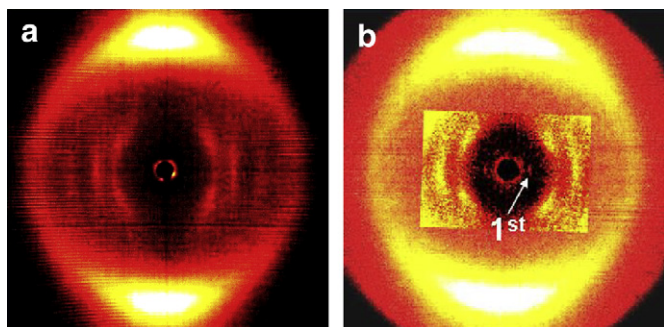


Fig. 8. 2D WAXD patterns of a PM6Az fiber recorded at 25 (a) and 85 °C (b). The fiber axis is along meridian. In (b), the contrast of the center part of low-angle diffraction is purposely increased, and the arrow indicates the first-order diffraction.

measured to be 16, 27, and 57%, respectively. For PMnAz ($n \geq 8$), the proton resonance band at $\delta = 1.27$ ppm of the backbone methyl groups in isotactic arrangements was overlapped by the resonance signal of protons from the center part of spacer, and thus the stereocomposition could not be calculated. However, the ^1H NMR still clearly indicated that the [rr] is rather high. The partial stereoregularity of PMnAz certainly facilitates the formation of mesogen domains. The 2D WAXD shown in Figs. 8b and 7 implies that the mesogen domains within the SmA layers of PM6Az are arranged in a more regular manner compared with those of PMnAz ($n \geq 8$). In our FT-IR experiments of the four samples at room temperature, the intensity ratio of the 1472 cm^{-1} band to 1467 cm^{-1} band was found to be increased with decreasing the

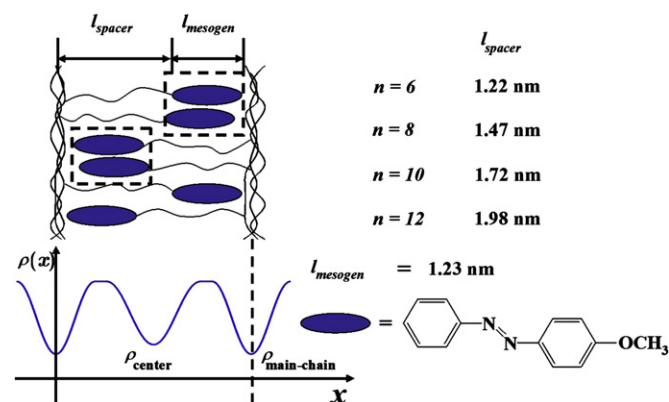


Fig. 9. Schematic draw of the fully interdigitated side-chain packing of the PMnAz SmA structure. l_{mesogen} is length of *p*-methoxyazobenzene; l_{spacer} is the spacer length calculated with an assumption that the alkyl spacer adopts an all-*trans* conformation. The lower part of the drawing shows the possible electron density profile along the smectic layer normal.

spacer length, indicating that the spacer of PM6Az possesses the highest *trans* content. This might be one of the reasons to account for the seemingly regular undulation of the mesogen domains in PM6Az.

It is well known that in solid state the azobenzene groups at close proximity may associate with each other to form aggregates with coplanar transition dipoles [23,40–45]. As the mesogen domains in the smectic layers of PMnAz are formed by the azobenzene groups from the same sublayer of main chain, we suspect that the H-aggregation is favored. It is of interest to investigate whether annealing of the samples in SmA phase will improve the H-aggregated azobenzene packing. In our DSC experiments of PM8Az, we found that after the sample was slowly cooled at a rate $\leq 2\text{ °C/min}$, an additional endothermic peak appeared right after the glass transition on the heating trace. For example, the heating trace of PM8Az recorded after a simple cooling from 160 °C at 1 °C/min [curve (a) in Fig. 11] demonstrates

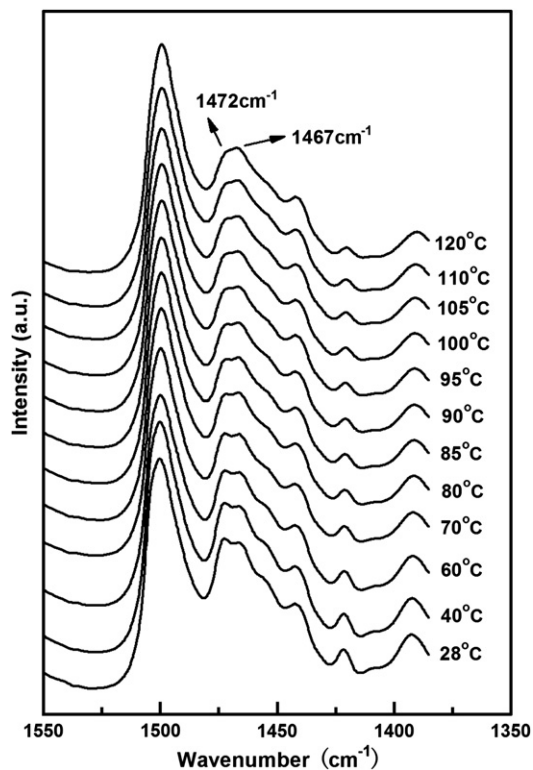


Fig. 10. A set of FT-IR spectra of a PM8Az film obtained at different temperatures upon heating. At each temperature, the sample was stayed isothermally for 10 min before taking the measurement.

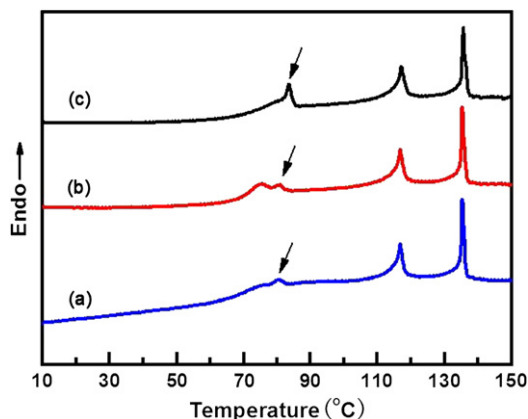


Fig. 11. A set of DSC heating traces of PM8Az at a rate of 2.5 °C/min. The samples were first cooled from 160 °C at 1 °C/min. For (a), the heating was carried out immediately after cooling; for (b) and (c), the samples were further annealed at 60 and 75 °C for 3 h, respectively, before heating. The arrow indexes the additional endothermic peak that is related to the decomposition of H-aggregation.

a small peak at ~ 83 °C, which is different from the enthalpy relaxation peak at ~ 75 °C of PM8Az shown in Fig. 1. We found that this peak is annealing temperature dependent. As shown by curve (b) of Fig. 11, annealing of a slowly cooled sample (cooling rate of 1 °C/min) at 60 °C for 3 h clearly generates an endothermic hysteresis peak of glass transition, but hardly affects the peak at ~ 83 °C. On the other hand, annealing of PM8Az at 75 °C, which is 3 °C higher than its T_g , can make the peak much larger as shown by curve (c) in Fig. 11. Since the WAXD experiments confirmed that no phase transition of SmA occurred in the corresponding temperature range, most likely, this endotherm is associated with decomposition of the H-aggregation formed during slow cooling and/or annealing at a temperature slightly higher than T_g .

Fig. 12a shows a set of UV–vis spectra of PM8Az film obtained during annealing at 75 °C. To erase the thermal history, the film sample was first cooled from isotropic state. The UV absorption ranging from 275 to 425 nm in fact includes three peaks (pointed by the arrows in Fig. 12a) with absorption maxima at 326 nm for H-aggregated, 360 nm for nonassociated, and 382 nm for

J-aggregated chromophores, respectively [43,45]. While the other two peaks remain essentially unchanged, the peak at 326 nm is gradually developed with time, indicating that the more and more mesogens were packed face-to-face with an increased order [44,45]. In accordance with the DSC result shown by the curve (b) in Fig. 11, we found that annealing the sample at below T_g could not enhance the absorption band at 326 nm. This implies that the rearrangement of the azobenzene groups in fact also requires the main chains to be sufficiently mobile [26]. The development of H-aggregation will cause the contraction along the SmA layer. In this sense, although the mesogen and the backbone of PM8Az are well separated by a reasonably long flexible spacer, their motions are still coupled to a certain extent. The decomposition of annealing induced H-aggregation at 80–85 °C could be evidenced by the UV–vis experiment. Upon heating of the 75 °C annealed PM8Az film, the absorption band at 326 nm disappears abruptly at 85 °C as shown in Fig. 12b. It is suggested that increasing the *gauche* content of the alkyl spacers may trigger the rupture of H-aggregation [42]. In Fig. 10, FT-IR heating result of PM8Az, the apparent intensity of 1467 cm^{-1} band is found to exceed that of 1472 cm^{-1} at 85 °C. With more *gauche* conformation, the thermal motion of the spacer certainly becomes stronger, which may penetrate to the mesogen domain and thus break the annealing induced H-aggregation [46,47].

We found that whether the annealing at a temperature slightly higher than T_g can generate a more ordered H-aggregation is dependent on the spacer length of PM*n*Az. As shown by the UV–vis spectra in Fig. 13, annealing the PM10Az film at 73 °C (6 °C higher than its T_g) for a prolonged time (e.g. 16 h) can lead to a pronounced shoulder at 326 nm, similar to that observed for PM8Az. Upon heating, this absorption shoulder disappeared after 76 °C. Our DSC heating experiment of PM10Az could not detect an endotherm which could be clearly related to the cracking of H-aggregation. It might be due to that the decomposition process occurred in a temperature range overlapped with the hysteresis of glass transition of PM10Az. Moreover, it was also possible that the H-aggregation of PM10Az was not as well developed as that of PM8Az. Fig. 13 also includes the UV–vis spectra of the PM6Az and PM12Az films recorded before and after annealing. The annealing temperatures were selected to be 78 and 68 °C, respectively, for

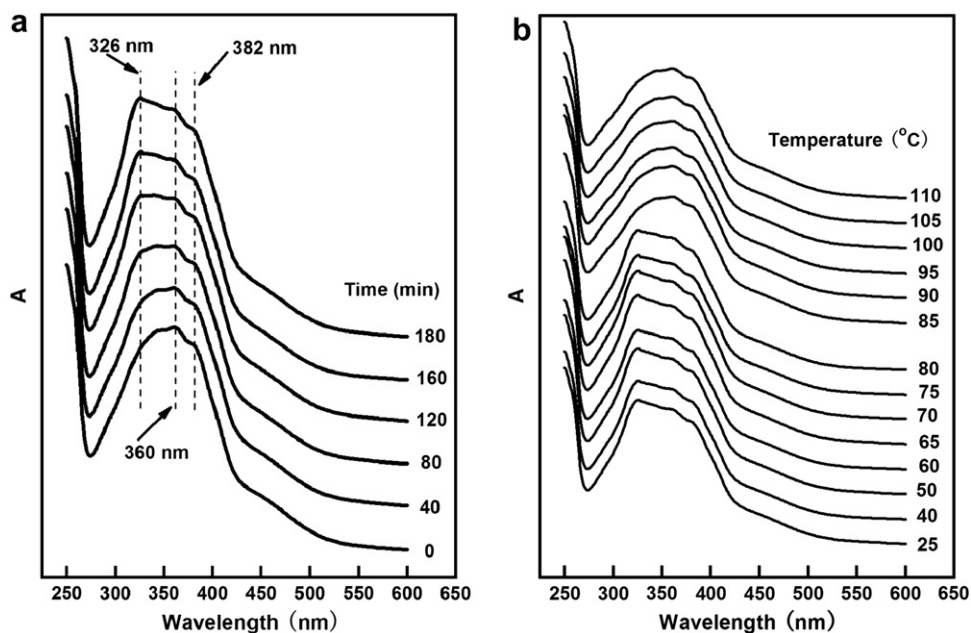


Fig. 12. UV–vis absorption spectra of PM8Az films (a) obtained at different times during annealing at 75 °C after the sample was cooled from 150 °C to room temperature at 1 °C/min, and (b) obtained at different temperatures upon heating after the sample was annealed at 75 °C for 3 h.

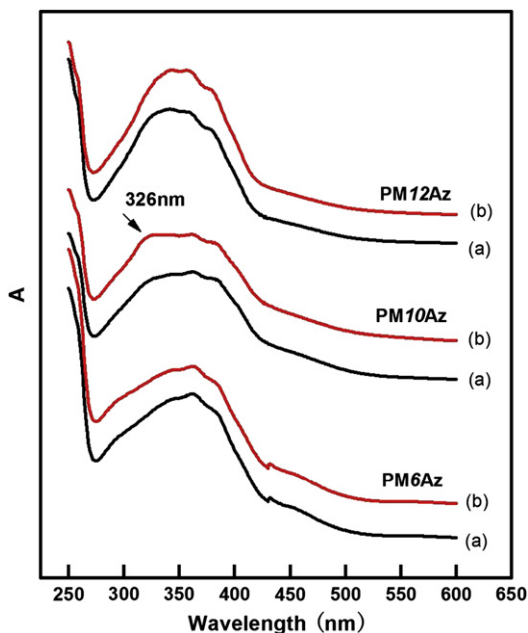


Fig. 13. UV-vis spectra of the PMnAz films with $n = 6, 10, 12$ recorded before (a) and after (b) annealing. For these three samples, the annealing temperatures were chosen to be 78, 73, and 68 °C, respectively.

PM6Az and PM12Az. For these two PMnAzs, the spectra of the annealed samples are nearly identical to those recorded right after cooling to room temperature from isotropic state. This indicates that annealing at the particular temperatures, which are ~ 4 °C higher than the corresponding T_g s, does not lead to a remarkable development of H-aggregation of PM6Az and PM12Az. We presume that the spacer of PM6Az might be too short to provide sufficient mobility for the azobenzene groups to rearrange in their domains. On the other hand, the high *gauche* content of the spacers in PM12Az may also disfavor the further development of H-aggregated azobenzene packing.

4. Conclusion

We have synthesized a series of side-chain LC poly-methacrylates based on *p*-methoxyazobenzenes (PMnAzs, $n = 6, 8, 10, 12$) with the apparent M_n of $\sim 10^5$ g/mol. Upon using different characterization techniques, the phase structures and transition behaviors of the polymers were carefully studied. The LC phase transition of PM6Az and PM8Az follows the sequence of SmA \leftrightarrow N \leftrightarrow I. PM10Az and PM12Az may adopt a similar transition sequence with an incomplete SmA-to-N transition during heating to isotropic state. Our WAXD experiments reveal that the layer periodicity of the low-temperature SmA phase is almost identical to the side-chain length of PMnAz. However, the first-order diffraction is much weaker than the second one, and only can be observed when the temperature approaches to the transition of SmA \leftrightarrow N. The absence of the first-order diffraction is most likely due to the electron density of the center portion of the side-chain sublayer matching with that of main-chain sublayer of the smectic structure. As the side chains were packed fully interdigitated and thus only the azobenzene groups from the same main-chain sublayer could stack together, a sort of density undulation appeared within the smectic layer. Among the four samples, PM6Az exhibited the strongest density undulation with some addition orders. Annealing PM8Az and PM10Az at a temperature slightly higher than their T_g could significantly enhance the UV absorption at 326 nm, indicating a further development of H-aggregation. On DSC heating traces of the annealed PM8Az, an additional endothermic event

appears at ~ 83 °C, corresponding to the decomposition of the annealing improved H-aggregation. For PM6Az and PM12Az, the UV-vis spectrum of the annealed sample is nearly identical to that without annealing. Therefore, the annealing effect on the development of H-aggregation is dependent on the spacer length.

Acknowledgement

This work was supported by the National Natural Science Foundation of China (Grant Nos. 20025414, 20374003, and 50573001).

Appendix. Supporting information

Tacticity measurement of PMnAzs based on ^1H NMR results. Supplementary data associated with this article can be found in the online version at doi:10.1016/j.polymer.2008.04.054.

References

- [1] Ikeda T, Mamiya JI, Yu YL. *Angew Chem Int Ed* 2007;46:506.
- [2] Finkelmann H, Nishikawa E, Pereira GG, Warner M. *Appl Phys Lett* 2001;87:15501.
- [3] Natansohn A, Rochon P. *Chem Rev* 2002;102:4139.
- [4] Ichimura K. *Chem Rev* 2000;100:1847.
- [5] Natansohn A, Rochon P, Ho MS, Barrett C. *Macromolecules* 1995;28:4179.
- [6] Barrett CJ, Natansohn AL, Rochon PL. *J Phys Chem* 1996;100:8836.
- [7] Yu YL, Nakano M, Ikeda T. *Nature* 2003;425:145.
- [8] Kawashima Y, Nakagawa M, Ichimura K, Seki T. *J Mater Chem* 2004;14:328.
- [9] Ubukata T, Hara M, Ichimura K, Seki T. *Adv Mater* 2004;16:220.
- [10] Yu HF, Okano K, Shishido A, Ikeda T, Kamata K, Komura M, et al. *Adv Mater* 2005;17:2184.
- [11] Bobrovsky A, Shibaev V. *Polymer* 2006;47:4310.
- [12] Uchida E, Kawatsuki N. *Polymer* 2006;47:2322.
- [13] Yu YL, Ikeda T. *Angew Chem Int Ed* 2006;45:5416.
- [14] Han M, Morino S, Ichimura K. *Macromolecules* 2000;33:6360.
- [15] Wolff D, Cackovic H, Krüger H, Rübner J, Springer J. *Liq Cryst* 1993;14:917.
- [16] Nikonorova NA, Borisova TI, Shibaev VP. *Macromol Chem Phys* 2000;201:226.
- [17] Andruzzi L, Altomare A, Ciardelli F, Solaro R, Hvilsted S, Ramanujam PS. *Macromolecules* 1999;32:448.
- [18] Altomare A, Andruzzi L, Ciardelli F, Gallot B, Solaro R. *Polym Int* 1998;47:419.
- [19] Li M, Zhou EL, Xu JP, Chen XF. *J Appl Polym Sci* 1996;60:2158.
- [20] Tian Y, Watanabe K, Kong X, Abe J, Iyoda T. *Macromolecules* 2002;35:3739.
- [21] Robello DR. *J Polym Sci* 1990;28:1.
- [22] Freiberg S, Lagugne-Labarthe F, Rochon P, Natansohn A. *Macromolecules* 2003;36:2680.
- [23] Cojocariu C, Rochon P. *Macromolecules* 2005;38:9526.
- [24] Walther M, Faulhammer H, Finkelmann H. *Macromol Chem Phys* 1998;199:223.
- [25] Davidson P. *Prog Polym Sci* 1996;21:893.
- [26] Han M, Ichimura K. *Macromolecules* 2001;34:82.
- [27] Han M, Ichimura K. *Macromolecules* 2001;34:90.
- [28] Uchida E, Shiraku T, Ono H, Kawatsuki N. *Macromolecules* 2004;37:5282.
- [29] Hore DK, Natansohn AL, Rochon PL. *J Phys Chem B* 2003;107:2197.
- [30] Angeloni AS, Caretti D, Chiellini E, Galli G, Altomare A, Solaro R, et al. *Liq Cryst* 1989;4:513.
- [31] Stewart D, Imrie CT. *Polymer* 1996;37:3419.
- [32] Nakano T, Hasegawa T, Okamoto Y. *Macromolecules* 1993;26:5494.
- [33] Craig AA, Imrie CT. *Macromolecules* 1995;28:3617.
- [34] Yamada M, Itoh T, Nakagawa R, Hirao A, Nakahama S-I, Watanabe J. *Macromolecules* 1999;32:282.
- [35] Dobb MG, Finkelmann H, Grebowicz J, McIntyre JE, Platé NA, Rehage G, et al. *Adv Polym Sci* 1984;60/61:146.
- [36] Wunderlich B, Möller M, Grebowicz J, Baur H. *Adv Polym Sci* 1988;87:90.
- [37] Davidson P, Keller P, Levelut AM. *J Phys* 1985;46:939.
- [38] Tsukruk V, Shilov V, Lipatov Yu. *Macromolecules* 1986;19:1308.
- [39] Zheng RQ, Chen EQ, Cheng SZD, Xie F, Yan D, He T, et al. *Macromolecules* 2000;33:5159.
- [40] Okuyama K, Ikeda N, Yokoyama S, Ochiai Y, Hamada Y, Shimomura M. *Chem Lett* 1988:1031.
- [41] Shimomura M, Hamada Y, Tajima N, Okuyama K. *J Chem Soc Chem Commun* 1989:232.
- [42] Taniike K, Matsumoto T, Sato T, Ozaki Y, Nakashima K, Iriyama K. *J Phys Chem* 1996;100:15508.
- [43] Menzel H, Weichart B, Schmidt A, Paul S, Knolls W, Stumpe J, et al. *Langmuir* 1994;10:1926.
- [44] Geue Th, Ziegler A, Stumpe J. *Macromolecules* 1997;30:5729.
- [45] Tong X, Cui L, Zhao Y. *Macromolecules* 2004;37:3101.
- [46] Craig AA, Imrie CT. *J Mater Chem* 1994;4:1705.
- [47] Imrie CT, Karasz FE, Attard GS. *Macromolecules* 1992;25:1278.